coatings

MDPI

Communication

Switchable Dual-Function Terahertz Metamaterial Device Based on Vanadium Dioxide

Mingjia Xing and Yunjie Teng *

School of Opto-electronic Engineering, Changchun University of Science and Technology, Changchun 130022, China
* Correspondence: tengyunjie@cust.edu.cn

Abstract: On the basis of the temperature-controlled phase change properties of vanadium dioxide (VO_2), a dual-functional terahertz metamaterial device is proposed. The device can be switched between an absorber and a polarization converter. Simulation results demonstrate that the device acts as a terahertz wave absorber when the VO_2 is in the metallic state, and the reflected extinction ratio is less than −15 dB in the frequency range between 1.07 and 1.19 THz. Moreover, the absorption performance is insensitive to polarization. When the VO_2 is in the insulated state, the device behaves as a polarization converter, which can convert line-polarized light to cross-polarized light. The polarization conversion rate of the device is over 90% in the frequency range between 1.43 and 1.51 THz. The proposed dual-functional metamaterial device with tunable and diverse functions has broad and potentially useful uses in areas such as terahertz detection, modulation, and switching.

Keywords: terahertz; metamaterial; vanadium dioxide; absorber; polarization conversion; tunable

check for updates

Citation: Xing, M.; Teng, Y. Switchable Dual-Function Terahertz Metamaterial Device Based on Vanadium Dioxide. *Coatings* **2023**, *13*, 753. https://doi.org/10.3390/coatings13040753

Academic Editors: Anna Palau and Maria Vittoria Diamanti

Received: 5 March 2023
Revised: 29 March 2023
Accepted: 3 April 2023
Published: 9 April 2023

Copyright: © 2023 by the authors. Licensee MDPI, Basel, Switzerland. This article is an open access article distributed under the terms and conditions of the Creative Commons Attribution (CC BY) license (https://creativecommons.org/licenses/by/4.0/).

1. Introduction

The terahertz band of electromagnetic waves demonstrates several attractive characteristics, including non-ionization, fingerprint spectrum, sensitivity to weak resonance, and strong penetration of nonpolar materials, which have promising applications in communication [1], sensing [2], and imaging [3]. Due to the lack of natural materials that can directly interact with terahertz waves, metamaterial-based multifunctional devices need to be created in order to boost the development of terahertz technology. Metamaterials are artificially invented sub-wavelength periodic composite structures that display unique physical properties not found in natural materials, such as perfect absorption [4], anomalous reflection [5], and negative refraction [6], due to their novel optical properties. Currently, metamaterials have been extensively applied in stealth technology [7], meta-lenses [8], antennas [9], and other areas. The performance of optical metamaterials is mainly determined by their structures, particularly the unit structure. For optical metamaterials with specific unit structure arrangements, their optical properties are usually stable. Metamaterials in combination with tunable materials can achieve rich and switchable multifunctional optical devices as metamaterial technology advances [10–12]. Vanadium dioxide (VO_2) is a metal oxide with the feature of phase change [13]. As an ideal tunable material, it displays the transition from the insulating state to the metallic state at 340 K [14–18]. At room temperature, VO_2 has a high resistivity and high insulation in its monoclinic crystal structure. When the temperature is higher than 340 K, the conductivity of VO_2 rises by four to five orders of magnitude in a narrow temperature range, transforming it into a cubic structure with metal properties. More importantly, the VO_2 phase change can be reversed, and at a temperature lower than 340 K, the conductivity of VO_2 will completely recover to its original state. In addition to temperature control, the phase change of VO_2 can also be realized through electrical stimulation, pressure, chemical doping, and other methods [19,20]. Therefore, the appearance of VO_2 material lays the foundation for realizing tunable multifunctional metamaterial devices.

Since the classic three-layer metamaterial absorber was put forward by Landy et al. in 2008 [21], numerous metamaterial absorbers have been proposed. In the early stages of research, most absorbers were narrowband and non-tunable. In 2017, a metamaterial functional device was proposed that could switch from a narrow absorption band to a wide absorption band by applying the phase change of VO_2 [22]. In the year 2018, a metamaterial device that could switch between broadband absorption at different frequency bands using VO_2 was reported [23]. In recent years, absorbers have gradually been combined with other functions by utilizing the tunable properties of different materials, such as perfect reflection [24], electromagnetic induction transparency [25], and polarization conversion. Based on the VO_2 structure, researchers have achieved switching between narrowband perfect and broadband absorption and polarization conversion [26,27]. However, improving performance during the functional switching process of metamaterials remains a significant challenge.

In the work, a dual-functional terahertz metamaterial device is proposed based on the temperature-controlled phase change properties of VO_2 material, which achieves the best performance known so far on the basis of a simple structure. When VO_2 is in the metallic state, the device exhibits a high extinction ratio of THz waves, with a reflection extinction ratio less than −15 dB in the range of 1.07–1.19 THz, and functions as a THz wave absorber with insensitive polarization dependence. When VO_2 is insulating, the device achieves a high polarization conversion efficiency of more than 90% in the range of 1.43–1.51 THz for incident linearly polarized light to cross-polarization conversion and serves as an efficient polarization converter. Currently, only a fixed spectrum or a single function can be achieved by the majority of metamaterial devices. The metamaterial proposed in this work has a simpler structure and better performance in both functions, with greater potential for applications in fields such as optoelectronic detection, thermal imaging, thermal emitters, and solar cells.

2. Device Design

The schematic diagram of the crystal cell structure for the VO_2-based switchable dual-functional terahertz metamaterial device is shown in Figure 1a. The metasurface structure is composed of five layers from the top down: the VO_2 square ring, the upper layer polyimide, the gold square aperture ring structure, the lower layer polyimide, and the gold reflection layer. The metal-dielectric-metal structure is commonly applied in the design of an absorber. The uppermost metal state of VO_2 with a symmetric structure can generate an electromagnetic reaction with the incident electromagnetic wave to realize perfect absorption, and the symmetric square ring structure also aids in the elimination of anisotropy. The dielectric loss material, the polyimide layer, acts as an intermediate layer to attenuate the incident terahertz waves entering the material to a certain extent. The gold aperture ring with an asymmetric structure is used to achieve polarization rotation, and the bottom layer employs a gold reflection layer with a thickness greater than the skin depth to prevent from transmitting electromagnetic waves. Moreover, the design of a fully covered metal reflection layer can effectively reduce processing difficulty. Through the optimization of the geometric parameters, the period of the crystal cell is P = 90 μm. Figure 1b shows the top view of the VO_2 square ring with its geometric parameters l_1 = 37 μm, l_2 = 5 μm, and d = 5 μm. Figure 1c shows the top view of the gold square aperture ring structure with its geometric parameters l_3 = 50 μm and w = 7 μm. Figure 1d shows the lateral view of the crystal cell, in which the thickness of the VO_2 square ring, polyimide layer, and gold layer are respectively t_1 = 0.2 μm, h = 7.5 μm, and t_2 = 0.2 μm.

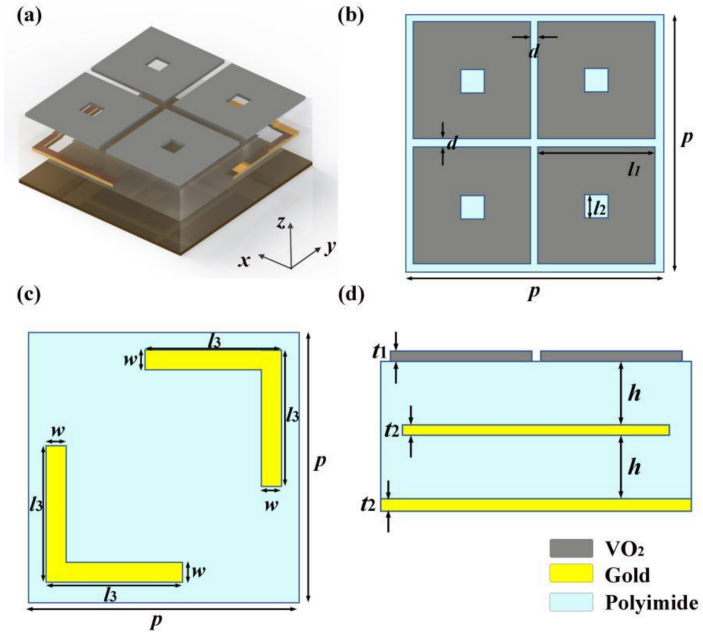


Figure 1. (**a**) The schematic diagram of the periodic cell structure of the metamaterial. (**b**) A top view of the VO_2 square-ring structure within the cell structure. (**c**) A top view of the gold aperture square-ring structure within the cell structure. (**d**) A side view of the cell structure.

The designed device was numerically simulated using the full-wave electromagnetic field simulation software CST with a frequency-domain solver. The crystal cell was set with a periodic boundary condition on the *x*- and *y*-axes and an open boundary condition on the *z*-axis. A *y*-polarized TE mode THz wave was normally incident on the surface of the unit structure along the -*z* direction. The phase change of VO_2 causes a big transmission in its conductivity, corresponding to different phases with different conductivities. When VO_2 is in the metallic state, its dielectric constant is usually described by the Drude model [28–31]. When in the insulating state, its dielectric constant is $\varepsilon_d = 9$. During simulation, the electrical conductivity of gold was set to 4.56×10^7 S/m [32], and the dielectric constant of polyimide was set to 3.5 with a loss tangent of 0.0027. In practice, a Janis cryostat whose temperature can be regulated by a resistance heater can be utilized to manage the device's overall temperature [33]. The device is fixed on the cold finger of the low-temperature thermostat, and a thermistor is mounted on the cold finger about 10 cm away from the device to monitor its temperature.

3. Results Analysis

3.1. Terahertz Wave Absorber

When VO_2 is in the metallic state, the operating state of the metasurface device is a terahertz absorber, mainly composed of the top VO_2 structure, polyimide layer, and gold reflection layer. The absorption rate is a vital parameter that indicates the performance of the absorber, and the calculation formula for the absorption rate is $A(\omega) = 1 - |S_{11}|^2 - |S_{21}|^2$, where $A(\omega)$ is the absorption rate, S_{11} is the reflection coefficient, and S_{21} is the transmission coefficient. Based on using a gold thin film with a thickness greater than the skin depth in the bottom layer of the structure in this work, the transmission coefficient of the absorber is $S_{21} = 0$, so the formula for the absorption rate can be simplified to $A(\omega) = 1 - |S_{11}|^2$. Figure 2a demonstrates the reflection coefficient of the designed absorber, which shows that the designed absorber has a reflection extinction ratio of less than -15 dB in the range of 1.07–1.19 THz, exhibiting excellent absorbing performance. There is a sharp absorption peak at $f = 1.13$ THz in the figure, with an absorption rate of 100%. To better understand the sensitivity of the designed terahertz absorber to polarization, we studied the changes in the device's reflection coefficient when TE and TM polarized incidence were applied.

As shown in Figure 2a, with the symmetry of the structure, the designed absorber shows superb polarization insensitivity. As a classical phase transition material, when VO_2 transits from an insulating state to a metallic state, the relationship between its conductivity and temperature can be expressed as $\sigma = -i\varepsilon_0\omega(\varepsilon_c - 1)$ [4,33,34], where σ is the conductivity, ε_0 is the vacuum permittivity, and ε_c is the dielectric constant of VO_2, which is temperature-dependent. Figure 2b shows the absorption spectra of the absorber corresponding to different conductivities of VO_2. When the conductivity of VO_2 transits from 200 S/m to 2×10^5 S/m, the absorption rate of the absorber rises from 5.9% to 100%.

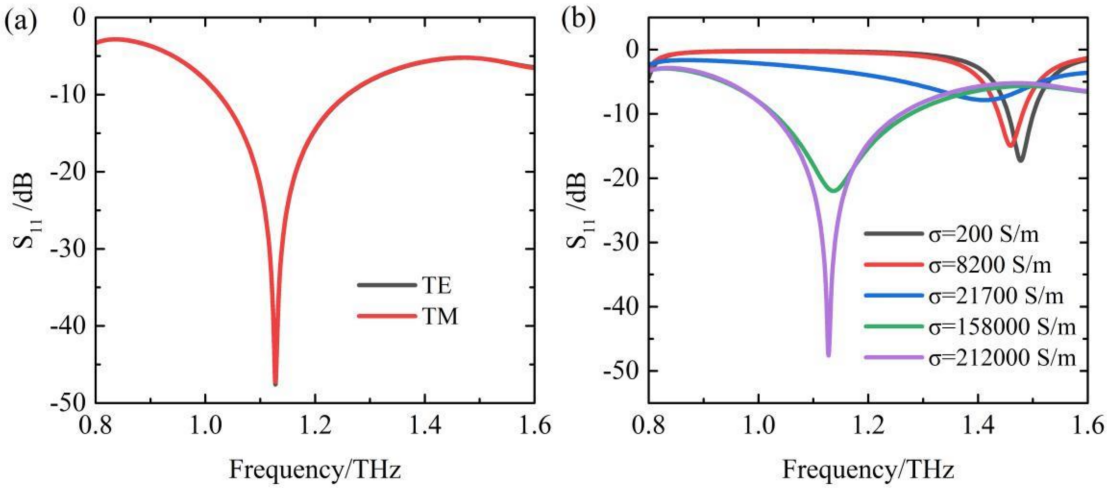


Figure 2. (**a**) Relation between the reflection coefficient and frequency of the absorber under different polarized incidence; (**b**) relation between the reflection coefficient and frequency of the absorber under different VO_2 conductivities.

To further illustrate the physical mechanism of the designed high-performance absorber, Figure 3 shows the electric field distribution at different frequencies above the VO_2 square ring structure in the absorber's *xy* plane. It can be observed that, at the resonant frequency of f = 1.13 THz, the energy is mainly concentrated in the gap between adjacent rings, whereas at frequencies outside the resonant frequency, such as f = 0.8 THz and f = 1.4 THz, the energy in the gap between adjacent rings is not concentrated. This indicates that the absorption effect of the absorber is mainly due to the strong coupling between adjacent unit cells. For frequencies f = 1.13 THz, since the concentrated energy is in the medium between the adjacent square rings, the coupling of the adjacent square rings caused the absorption. What's more, as for resonant frequencies, energy is concentrated in a parallel pattern to the electric field, which demonstrates that the electric dipole resonance is excited. According to the power distribution at the absorption peak, the author concluded that the absorption is caused by electric dipole resonance.

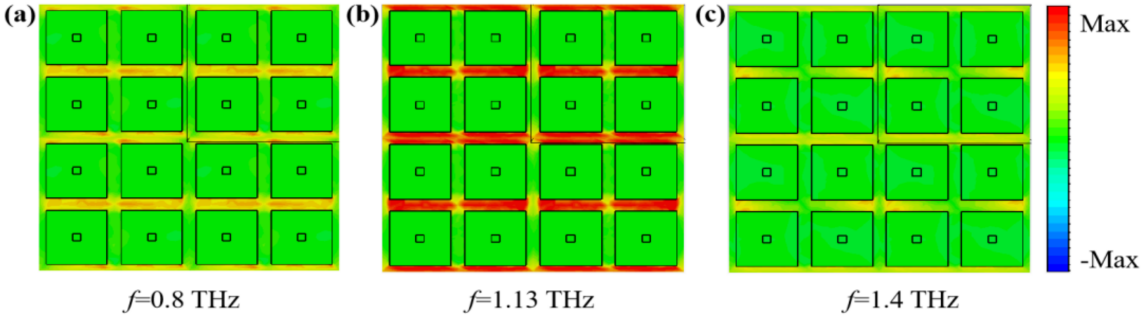


Figure 3. Electric field distribution on the VO_2 square ring structure at (**a**) 0.8 THz, (**b**) 1.13 THz, and (**c**) 1.4 THz frequencies.

In Figure 4, to investigate geometric parameters' influence on the structural metamaterial on the absorption rate, we calculated the impact of the VO_2 square ring width l_1 and the hole width l_2 on the absorber's absorption performance. Figure 4a indicates that with the increase of l_1, the absorption peak shifts towards lower frequencies, while the absorption rate changes and reaches a maximum at l_1 = 37 µm. Figure 4b indicates that as l_2 increases, the central frequency remains unchanged and the absorption rate increases, reaching a maximum at l_2 = 5 µm.

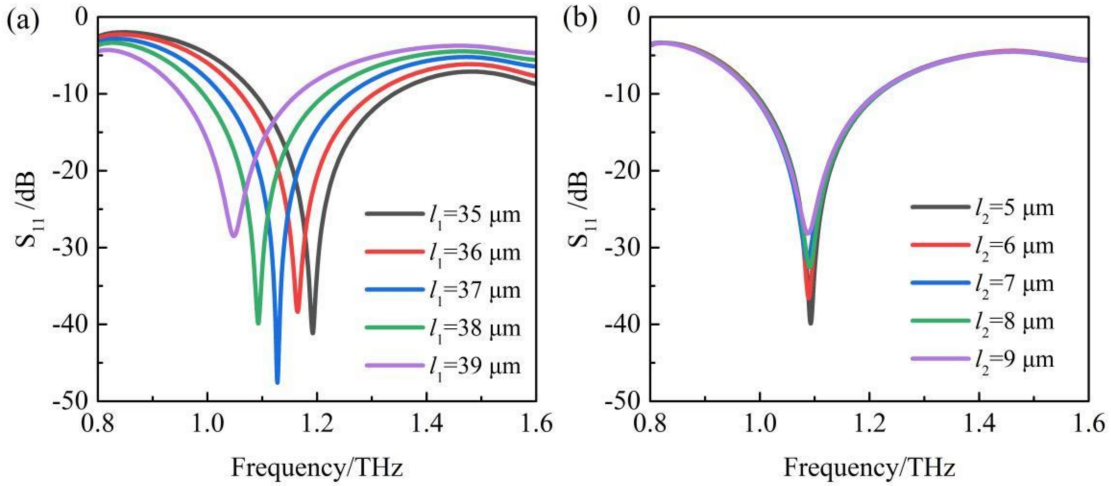


Figure 4. (**a**) Relation between the reflection coefficient and frequency of the absorber for different widths (l_1) of the VO_2 square ring resonator. (**b**) Relation between the reflection coefficient and frequency of the absorber for different hole widths (l_2) of the VO_2 square ring resonator.

3.2. Terahertz Wave Polarization Converter

When VO_2 is in the insulating state, the metasurface device, mainly achieved through the gold square aperture ring structure, polyimide layer, and gold reflection layer, works as a terahertz wave polarization converter. As shown in Figure 5a, due to the anisotropic characteristics of the gold square aperture ring structure, the incident *y*- and *x*-polarized wave can be resolved into two orthogonal components on the *u*- and *v*-axis, and it will stir up a resonance in the *u*- and *v*-axis directions with a phase difference of $\pm\pi/2$ or $\pm\pi$ between them, thereby realizing the cross-linear polarization conversion. Generally, assuming that the normal incident wave is y-polarized, the reflected electromagnetic wave can be expressed as: $\vec{E_r} = r_{xy}A_y\cos(\varphi_{xy})\vec{e_x} + r_{yy}A_y\cos(\varphi_{yy})\vec{e_y}$ where r_{xy} and r_{yy} are the reflection coefficients for *y*-to-*x* and *y*-to-*y* polarization conversions, respectively. To characterize the polarization conversion capability of the proposed device, the efficiency of the polarization converter can be expressed as $PCR = |r_{xy}|^2/\left(|r_{xy}|^2 + |r_{yy}|^2\right)$. To precisely determine the polarization of the reflected wave, Figure 5a demonstrates the change of the reflection coefficients r_{xy} and r_{yy} with frequency. At 1.47 THz, r_{xy} and r_{yy} are approximately 1 and 0, respectively, indicating that almost only x-polarized terahertz waves are near this frequency. Figure 5b shows the conversion efficiency of the polarization converter. It can be seen that the conversion efficiency is over 90% within the limit of 1.43–1.51 THz. The working broadband of polarization conversion is determined by the threshold range where the conversion efficiency is greater than 90%, indicating that almost all incident waves within this limit can be transformed into cross-polarized waves.

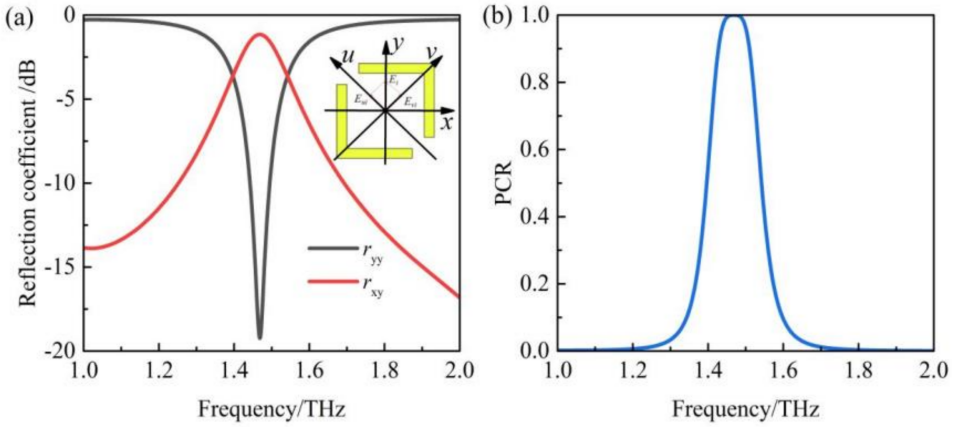


Figure 5. The relation between the reflection coefficient (**a**) and polarization conversion efficiency (**b**) of the polarization converter and frequency.

With the aim of further investigating the cross-polarization conversion mechanism of the converter, we ran the simulation that showed the surface current distribution of the polarization converter at different frequencies on the *xy* plane, as shown in Figure 6. It can be observed that the current distribution on the metal surface is not concentrated outside the resonant frequency (f = 1.0 THz or 2.0 THz). However, near the resonant frequency f = 1.47 THz, the concentration of the surface current mainly occurs on the gold square aperture ring structure, and the current vector direction on the gold square aperture ring structure (shown as the blue arrow in Figure 6b) is parallel and opposite to that on the surface of the gold substrate (shown as the black arrow in Figure 6b), forming a magnetic resonance. Efficient cross-polarization conversion can be achieved through the strong electromagnetic coupling effect.

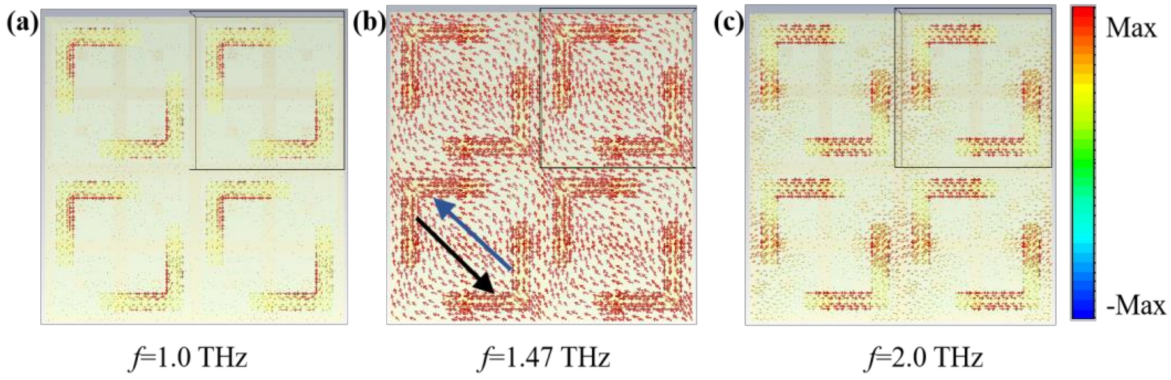


Figure 6. Surface current distribution on the gold square aperture ring structure at (**a**) 1 THz, (**b**) 1.47 THz, and (**c**) 2 THz frequencies.

In addition, we also analyzed the effects of the gold square aperture ring structure parameters, l_3 and w, on the device's polarization conversion performance. Figure 7a shows that as l_3 rises gradually, the center frequency of PCR redshifts, while the maximum conversion efficiency remains constant. As shown in Figure 7b, as w increases, the operating bandwidth increases, the center frequency remains constant, and the maximum conversion efficiency remains constant.

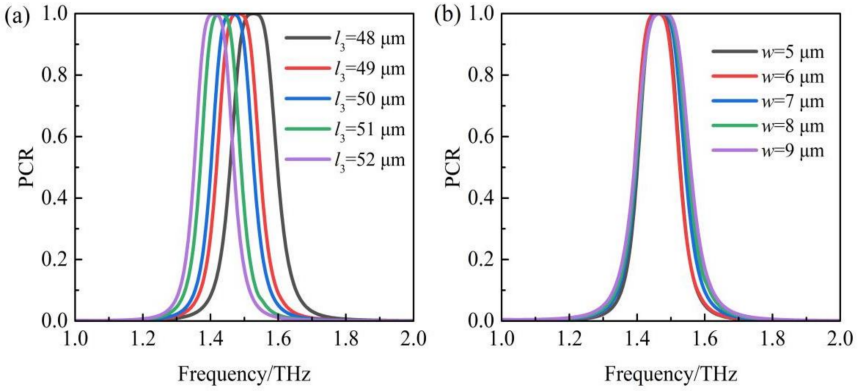


Figure 7. (**a**) Polarization conversion efficiency of the device with gold square aperture ring structure with parameter l_3; (**b**) polarization conversion efficiency of the device with gold square aperture ring structure with parameter w.

4. Conclusions

In general, based on the temperature-controlled phase change properties of VO_2 material, a dual-functional terahertz metamaterial device has been proposed in this paper that can switch between absorber and polarization converter functions. Simulation results show that when VO_2 is in its metallic state, the device functions as a terahertz wave absorber with a reflectivity extinction ratio of less than −15 dB in the range of 1.07–1.19 THz, demonstrating good absorption performance and insensitivity to polarization. When VO_2 is in its insulating state, the device behaves as a polarization converter, with a cross-linear polarization conversion efficiency of over 90% in the range of 1.43–1.51 THz. The designed dual-functional metamaterial device is characterized by tunability and diversity, providing creative ways to create a fast-response active terahertz wave modulator.

Author Contributions: Writing—original draft and investigation, M.X. and Y.T.; Data analysis and derived formula, M.X.; Funding acquisition, Y.T.; Experiment setup and data analysis guiding, M.X. All authors have read and agreed to the published version of the manuscript.

Funding: Department of Science and Technology of Jilin province: No.20220201074GX;Jilin Provincial Department of Education Scientific Research Project: JJKH20220750KJ.

Institutional Review Board Statement: Not applicable.

Informed Consent Statement: Not applicable.

Data Availability Statement: Not applicable.

Conflicts of Interest: The authors declare no conflict of interest.

References

1. Rappaport, T.S.; Xing, Y.; Kanhere, O.; Ju, S.; Madanayake, A.; Mandal, S.; Alkhateeb, A.; Trichopoulos, G.C. Wireless communications and applications above 100 ghz: Opportunities and challenges for 6G and beyond. *IEEE Access* **2019**, *7*, 78729–78757. [CrossRef]
2. Singh, R.; Al-Naib, I.A.; Koch, M.; Zhang, W. Sharp fano resonances in thz metamaterials. *Optics Express* **2011**, *19*, 6312–6319. [CrossRef] [PubMed]
3. Stantchev, R.I.; Yu, X.; Blu, T. Pickwell-MacPherson E., Real-time terahertz imaging with a single-pixel detector. *Nat. Commun.* **2020**, *11*, 2535. [CrossRef] [PubMed]
4. Zhang, Y.; Wu, P.; Zhou, Z.; Chen, X.; Yi, Z.; Zhu, J.; Zhang, T.; Jile, H. Study on temperature adjustable terahertz metamaterial absorber based on vanadium dioxide. *IEEE Access* **2020**, *8*, 85154–85161. [CrossRef]
5. Sun, S.; Yang, K.Y.; Wang, C.M.; Juan, T.K.; Chen, W.T.; Liao, C.Y.; He, Q.; Xiao, S.; Kung, W.T.; Guo, G.Y.; et al. High-efficiency broadband anomalous reflection by gradient meta-surfaces. *Nano Lett.* **2012**, *12*, 6223–6229. [CrossRef]
6. Ramakrishna, S.A. Physics of negative refractive index materials. *Rep. Progr. Phys.* **2005**, *68*, 449–521. [CrossRef]
7. Liu, Y.; Li, Z.; Zhang, W.; Sun, Y. Design and emulation of combined-shaped electromagnetic stealthy cloak made of metamaterial. *J. Funct. Mater.* **2013**, *44*, 2235–2238.

8. Shen, N.H.; Foteinopoulou, S.; Kafesaki, M.; Koschny, T.; Ozbay, E.; Economou, E.N.; Soukoulis, C.M. Compact planar far-field superlens based on anisotropic left-handed metamaterials. *Phys. Rev. B* **2009**, *80*, 115123. [CrossRef]
9. Zhu, J.; Eleftheriades, G.V. A compact transmission-line metamaterial antenna with extended bandwidth IEEE Antennas Wirel. *Propag. Lett.* **2009**, *8*, 295–298.
10. Bilal, R.M.; Naveed, M.A.; Baqir, M.A.; Ali, M.M.; Rahim, A.A. Design of a wideband terahertz metamaterial absorber based on Pythagorean-tree fractal geometry. *Opt. Mater. Express* **2020**, *10*, 3007. [CrossRef]
11. Naveed, M.A.; Bilal, R.M.; Rahim, A.A.; Baqir, M.A.; Ali, M.M. Polarization-insensitive dual-wideband fractal meta-absorber for terahertz applications. *Appl. Opt.* **2021**, *60*, 9160–9166. [CrossRef]
12. Yan, D.; Wang, Y.; Qiu, Y.; Feng, Q.; Li, X.; Li, J.; Qiu, G.; Li, J. A review: The functional materials-assisted terahertz metamaterial absorbers and polarization converters. *Photonics* **2022**, *9*, 335. [CrossRef]
13. Verleur, H.W.; Barker, A.S.; Berglund, C.N. Optical properties of VO2 between 0.25 and 5 eV. *Phys. Rev.* **1968**, *172*, 788–798. [CrossRef]
14. Morin, F.J. Oxides which show a metal-to-insulator transition at the neel temperature. *Phys. Rev. Lett.* **1959**, *3*, 34–36. [CrossRef]
15. Jeong, Y.G.; Han, S.; Rhie, J.; Kyoung, J.S.; Choi, J.W.; Park, N.; Hong, S.; Kim, B.J.; Kim, H.T.; Kim, D.S. A vanadium dioxide metamaterial disengaged from insulator-tometal transition. *Nano Lett.* **2015**, *15*, 6318–6323. [CrossRef]
16. Liu, L.; Kang, L.; Mayer, T.S.; Werner, D.H. Hybrid metamaterials for electrically triggered multifunctional control. *Nature Commun.* **2016**, *7*, 13236. [CrossRef]
17. Budai, J.D.; Hong, J.; Manley, M.E.; Specht, E.D.; Li, C.W.; Tischler, J.Z.; Abernathy, D.L.; Said, A.H.; Leu, B.M.; Boatner, L.A.; et al. Metallization of vanadium dioxide driven by large phonon entropy. *Nature* **2014**, *515*, 535. [CrossRef]
18. Hilton, D.J.; Prasankumar, R.P.; Fourmaux, S.; Cavalleri, A.; Brassard, D.; El Khakani, M.A.; Kieffer, J.C.; Taylor, A.J.; Averitt, R.D. Enhanced photosusceptibility near Tc for the light-induced insulator-to-metal phase transition in vanadium dioxide. *Phys. Rev. Lett.* **2007**, *99*, 226401. [CrossRef]
19. Ruzmetov, D.; Gopalakrishnan, G.; Deng, J.D.; Narayanamurti, V.; Ramanathan, S. Electrical triggering of metal–insulator transition in nanoscale vanadium oxide junctions. *J. Appl. Phys.* **2009**, *106*, 083702. [CrossRef]
20. Tian, X.; Li, Z.-Y. An optically-triggered switchable mid-infrared perfect absorber based on phase-change material of vanadium dioxide. *Plasmonics* **2018**, *13*, 1393–1402. [CrossRef]
21. Landy, N.I.; Sajuyigbe, S.; Mock, J.J.; Smith, D.R.; Padilla, W.J. Perfect metamaterial absorber. *Phys. Rev. Lett.* **2008**, *100*, 207402. [CrossRef] [PubMed]
22. Liu, Z.J.; Zhao, M.Y.; Gao, J.; Li, Y.S.; Jiang, S.H. Thermally tunable broadband omnidirectional and polarization-independent super absorber using phase change material VO_2. *Results Phys.* **2017**, *7*, 4222–4225. [CrossRef]
23. Zhao, Y.; Huang, Q.P.; Cai, H.L.; Lin, X.X.; Lu, Y.L. A broadband and switchable VO_2-based perfect absorber at the THz frequency. *Opt. Commun.* **2018**, *426*, 443–449. [CrossRef]
24. Dao, R.N.; Kong, X.R.; Zhang, H.F.; Su, X.R. A tunable broadband terahertz metamaterial absorber based on the vanadium dioxide. *Optik* **2019**, *180*, 619–625. [CrossRef]
25. Song, Z.Y.; Zhang, B.C. Controlling wideband absorption and electromagnetically induced transparency via a phase change material. *Europhys. Lett.* **2020**, *129*, 57003. [CrossRef]
26. He, H.; Shang, X.; Xu, L.; Zhao, J.; Cai, W.; Wang, J.; Zhao, C.; Wang, L. Thermally switchable bifunctional plasmonic metasurface for perfect absorption and polarization conversion based on VO_2. *Opt. Express* **2020**, *28*, 4563–4570. [CrossRef]
27. Song, Z.; Zhang, J. Achieving broadband absorption and polarization conversion with a vanadium dioxide metasurface in the same terahertz frequencies. *Opt. Express* **2020**, *28*, 12487–12497. [CrossRef]
28. Song, Z.; Deng, Y.; Zhou, Y.; Liu, Z. Terahertz toroidal metamaterial with tunable properties. *Opt. Express* **2019**, *27*, 5792–5797. [CrossRef]
29. Wang, S.; Kang, L.; Werner, D.H. Hybrid resonators and highly tunable terahertz metamaterials enabled by vanadium dioxide (VO_2). *Sci. Rep.* **2017**, *7*, 4326. [CrossRef]
30. Matsui, H.; Ho, Y.L.; Kanki, T.; Tanaka, H.; Delaunay, J.J.; Tabata, H. Mid-infrared plasmonic resonances in 2D VO_2 nanosquare arrays. *Adv. Opt. Mater.* **2015**, *3*, 1759–1767. [CrossRef]
31. Liu, M.; Hwang, H.Y.; Tao, H.; Strikwerda, A.C.; Fan, K.; Keiser, G.R.; Sternbach, A.J.; West, K.G.; Kittiwatanakul, S.; Lu, J.; et al. Terahertz-field-induced insulator-to-metal transition in vanadium dioxide metamaterial. *Nature* **2012**, *487*, 345–348. [CrossRef]
32. Jiao, X.F.; Zhang, Z.H.; Li, T.; Xu, Y.; Song, G.F. Tunable dual broadband terahertz metamaterial absorber based on vanadium dioxide. *Appl. Sci.-Basel.* **2020**, *10*, 7259. [CrossRef]
33. Li, H.; Peng, H.; Ji, C.; Lu, L.; Li, Z.; Wang, J.; Wu, Z.; Jiang, Y.; Xu, J.; Liu, Z. Electrically tunable mid-infrared antennas based on VO_2. *J. Mod. Opt.* **2018**, *65*, 1809–1816. [CrossRef]
34. Chen, X.-S.; Li, J.-S. Tunable terahertz absorber with multi-defect combination embedded VO_2 thin film structure. *Acta Phys. Sin.* **2020**, *69*, 027801. [CrossRef]

Disclaimer/Publisher's Note: The statements, opinions and data contained in all publications are solely those of the individual author(s) and contributor(s) and not of MDPI and/or the editor(s). MDPI and/or the editor(s) disclaim responsibility for any injury to people or property resulting from any ideas, methods, instructions or products referred to in the content.